Study of the distribution of the molecular orientation in thick polyethylene samples by X-ray diffraction, infra-red dichroism and Raman spectroscopy

Claude-Paul Lafrance, Paul Chabot, Marie Pigeon, Robert E. Prud'homme and Michel Pézolet*

Centre de Recherche en Sciences et Ingénierie des Macromolécules, Département de Chimie, Université Laval, Québec, Canada G1K 7P4

(Received 3 December 1992)

The molecular orientation in thick polyethylene samples has been studied by wide-angle X-ray diffraction, i.r. dichroism and Raman spectroscopy. The original specimens, with dimensions of the order of a centimetre, were cut to obtain 1 mm thick platelets on which the measurements were made. The mean coefficient of the second-order Legendre polynomial, $\langle P_2 \rangle$, was calculated from X-ray diffraction and from the 1894 cm^{-1} i.r. band for the crystalline phase, from the 909 cm^{-1} i.r. band for the vinyl end groups and from the 1130 and 1060 cm^{-1} Raman bands for the all-*trans* C–C conformers. The fourth-order coefficient, $\langle P_4 \rangle$, was also determined from X-ray diffraction and Raman spectroscopy for a series of cylindrical rods of draw ratios (λ) ranging from 6 to 20. An excellent correlation is observed between the $\langle P_2 \rangle$ coefficients measured from different X-ray reflections and from the 1894 cm^{-1} i.r. band. The Raman spectroscopy results show that the all-*trans* bonds located in the amorphous phase are aligned perpendicular to the extrusion direction for the $\lambda = 6$ rod, and gradually reorient towards the fibre axis for λ values up to 20, while the $\langle P_2 \rangle$ and $\langle P_4 \rangle$ coefficients calculated for the crystalline phase remain constant at $\lambda \geqslant 12$. The variation of the orientation through the thickness of the samples was investigated for the cylindrical rods and for an H-shaped moulding produced by extrusion and rolling. Minor differences in the degree of molecular orientation were detected between the centre and the surface of the rods, whereas important variations were measured for the H-shaped sample.

(Keywords: X-ray diffraction; infra-red dichroism; Raman spectroscopy)

INTRODUCTION

The deformation of thermoplastics induces the alignment of the molecular chains along the elongation direction, which results in an increase in the strength of the material in this direction[1,2]. Industrial processes such as melt spinning, injection moulding, blow moulding and tubular film extrusion take advantage of the enhanced mechanical properties[2–4]. In these processes, the polymer is extruded in the molten state and the major part of the deformation occurs prior to its solidification. However, the degree of orientation depends on the stress at the time of solidification and is usually low. In order to obtain higher orientation, polymers have to be deformed in their solid state, by drawing, rolling or extrusion, which is achieved in a second step in industrial processing[2]. Until now, only fibres and thin films ($\leqslant 0.2$ mm) have been produced in a highly oriented state, but thick sheets, rods and profiled beams may be predicted to be promising new polymeric materials.

The characterization of oriented polymers involves the evaluation of their degree of orientation, which provides a measure of the width of the distribution of the structural units with respect to the macroscopic axis of the sample, and the determination of the type of orientation distribution[1,2,5]. Uniaxial orientation corresponds to the alignment of the molecular chains in one direction, as is obtained, for example, in the drawing of fibres. In the case of uniaxial orientation with cylindrical symmetry, the chain axis is oriented in the deformation direction (DD, *Figure 1*), while other axes defined by different structural units of the polymer (i.e. other crystal axes)

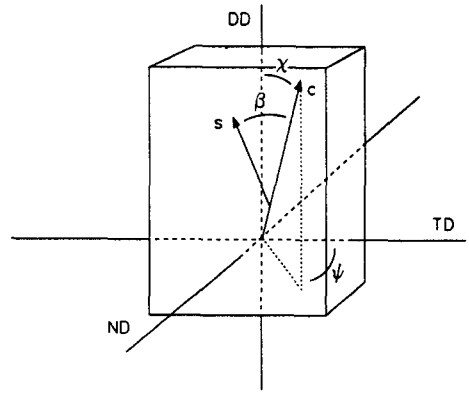

Figure 1 Angles χ and ψ defining the position of the crystallographic *c*-axis, or molecular chain axis, *c*, with respect to the deformation, transverse and normal directions (DD, TD and ND, respectively), and angle β between a given structural unit, *s*, and the molecular chain axis

* To whom correspondence should be addressed

0032-3861/93/245029-09

show random orientation about this direction. Double orientation is found when the chain axis is aligned along the DD and other crystal axes also possess preferred orientations. Double orientation has been reported to occur in rolled polyethylene (PE)[6–8] and polypropylene[9], and in drawn crystal mats of ultra-high molecular weight PE (UHMWPE)[10–14]. Biaxial orientation is generally used to designate the state of a material showing enhanced mechanical properties in two directions. In most cases, biaxial orientation corresponds to a broad orientation distribution of the molecular chains in one plane, and it has been shown that the drawing of UHMWPE in two directions perpendicular to each other leads to the formation of an interwoven fibrillar network[10–12].

Different techniques can be used to measure the orientation of polymer structural units[1,2,15,16]. Some methods give information on the overall orientation in the sample, while others can be used to measure the orientation in either the crystalline or amorphous phases of the material, or sometimes in both phases. So far, most studies of the orientation in polymers have been performed on specimens having a thickness of <0.2 mm. The characterization of molecular orientation in thick samples requires some modifications of the experimental procedures developed for thin samples. In many instances, the use of a sectioning technique is necessary because of the size and shape of the specimens, particularly with characterization methods such as birefringence, i.r. dichroism or Raman spectroscopy, which require transparent samples. However, it is also necessary to assess the influence of the sectioning technique on the orientation of the material. The characterization of a three-dimensional sample is further complicated by the inhomogeneity of the orientation through its thickness. In the simplest case, there may be a gradient in the degree of uniaxial orientation from the interior to the exterior of the material. For specimens possessing a complex shape, biaxial or double orientation may be expected to occur, as well as transition zones exhibiting a sharp variation of orientation near the bends. The characterization of such samples requires the determination of a topographical map describing the variation of the orientation through their thickness.

In this work, three different techniques have been used to characterize completely the orientation of thick extruded samples of PE. Wide-angle X-ray diffraction (WAXD) has allowed the determination of the orientation of the three crystallographic axes, while Raman spectroscopy and i.r. dichroism have been used to study the orientation of different segments of the PE chains in the amorphous and crystalline phases. The orientation was measured in samples cut from uniaxially extruded cylindrical rods and from an H-shaped moulding prepared by extrusion and rolling. An orientation topographical map was determined for this latter moulding, since important variations were detected from the edges to the centre of the sample. The results obtained by the three characterization methods will be compared, and the influence of the sectioning technique will be discussed.

THEORY

The orientation of a sample at the macroscopic level is the average orientation of each of its structural units. For a uniaxially oriented sample, if the molecular chains exhibit a cylindrical symmetry around the DD (*Figure 1*), the orientation distribution of the molecular chains, $N(\chi)$, can be described[1,2,15,16] as a function of the polar angle χ only, using a series of even order Legendre polynomials $P_n(\cos\chi)$:

$$N(\chi)=\sum_{n=0}^{\infty}(n+1/2)\langle P_n(\cos\chi)\rangle P_n(\cos\chi) \qquad (1)$$

The orientation in a sample can thus be expressed in terms of the $\langle P_n(\cos\chi)\rangle$ coefficients that characterize the distribution. The zeroth coefficient corresponds to the isotropic case, and is therefore equal to unity for all orientations. The second-order coefficient is the well-known 'Hermans orientation function'[17,18]:

$$\langle P_2\rangle\equiv\langle P_2(\cos\chi)\rangle=(3\langle\cos^2\chi\rangle-1)/2 \qquad (2)$$

In this paper, the notation $\langle P_n\rangle$ will be used to represent the mean coefficient of the nth-order Legendre polynomial. The angular brackets indicate that an average is taken over all orientations in the sample. For a given structural unit, $\langle P_2\rangle$ takes the value -0.5 or 1.0 when all units are oriented perpendicular or parallel to the DD, respectively, while it equals zero in the case of random orientation. All methods used for the characterization of the molecular orientation allow for the determination of the second-order coefficient, $\langle P_2\rangle$. Some methods, such as Raman spectroscopy, enable the calculation of the fourth-order coefficient, $\langle P_4\rangle$, while the coefficients $\langle P_4\rangle$ to $\langle P_8\rangle$ can be determined by n.m.r. spectroscopy. WAXD is the only technique from which all the coefficients can be calculated. For samples of moderate draw ratios ($\lambda\leqslant 10$), the orientation can be described adequately by using only the second-order coefficient. For λ values >10, the $\langle P_2\rangle$ coefficient measured for the crystal phase becomes close to its limiting value and it is therefore necessary to use higher order coefficients in order to characterize the orientation distribution in such highly oriented samples[14,19].

I.r. dichroism

The dichroic ratio of a given i.r. absorption band is defined as $D=A_{\parallel}/A_{\perp}$, where $A_{\parallel}$ and $A_{\perp}$ are the absorbance of the band with the electric vector of the incident radiation polarized parallel and perpendicular to the DD, respectively. The second-order coefficient of the orientation distribution function is then given by[1,2,20]:

$$\langle P_2\rangle=\frac{(D-1)}{(D+2)} \qquad (3)$$

The coefficient characterizing the molecular chain orientation, $\langle P_2\rangle_c$, can be obtained by using:

$$\langle P_2\rangle_c=\frac{\langle P_2\rangle}{P_2(\cos\beta)}=\langle P_2\rangle\frac{(D_0+2)}{(D_0-1)} \qquad (4)$$

where $P_2(\cos\beta)$ is the value of the second-order Legendre polynomial and $D_0=2\,\mathrm{cotg}^2\beta$, β being the angle between the transition moment of the studied vibration and the chain axis (*Figure 1*).

In comparison with i.r. transmittance measurements of orientation for thin samples (typically 10–100 μm), absorption bands with low extinction coefficient have to be studied with thick specimens. In this work, the characterization of ~ 1 mm thick PE platelets by i.r. transmission spectroscopy was made from the 909 and

1894 cm^{-1} bands. The 1894 cm^{-1} band arises from a combination mode between the Raman and the i.r. active CH_2 rocking vibration, and is due to the crystalline phase only, while the 909 cm^{-1} band is associated with the CH_2 wagging vibration of the vinyl end groups. For both vibrations, the angle β between the transition moment vector and the molecular chain axis was taken as 90°[20,21].

Raman spectroscopy

Bower has developed a general theory for the determination by polarized Raman spectroscopy of the molecular orientation in polymers[22,23]. The Raman scattering intensity I_s is given by a quadratic expression of all the α_{ij} (i, j = D, T and N directions), the components of the Raman tensor for the studied vibration, with coefficients that are the direction cosines I_i and I'_j defining the polarization directions of the incident light and of the analyser with respect to the D, T and N axes fixed in the sample, respectively:

$$I_s = I_0 \sum (\sum I_i I'_j \alpha_{ij})^2 \quad (5)$$

where I_0 depends on instrumental factors and incident light intensity. The experimental values are thus of the form $I_0 \sum \alpha_{ij}\alpha_{pq}$ and, as the summation implies that all the scattering units contributing to the observed intensity are taken into account, they contain information about their distribution of orientations. Each α_{ij} can be expressed as a linear combination of the principal components α_D, α_T and α_N of the derived polarizability tensor and the Euler angles defining the orientation of the principal axes of the tensor with respect to the axes DD, TD and ND of the sample.

In the case of uniaxial cylindrical symmetry, with no preferred orientation about the chain axis, and with one of the tensor axes coincident with this axis (*Figure 1*, $\beta = 0°$)[20,22,23]:

$$\sum \alpha_{ij}\alpha_{pq} = 4\pi^2 N_0 \sum M_{n00} A_{n00}^{ijpq} \quad (6)$$

where N_0 is the number of structural units contributing to the Raman intensity and A_{n00}^{ijpq} is a sum of quadratic terms in α_D, α_T and α_N previously tabulated by Bower[22]. The $\langle P_2 \rangle$ and $\langle P_4 \rangle$ coefficients can then be calculated by:

$$\langle P_n \rangle = 4\pi^2 M_{n00} (n + \tfrac{1}{2})^{-1/2} \quad (7)$$

In comparison with other techniques that use the transmission geometry, Raman spectroscopy, which is a light scattering technique, should be insensitive to the thickness of the sample. However, incident or scattered light depolarization may occur for birefringent or light diffusing samples.

The 1130 and the 1060 cm^{-1} bands were used to study the orientation of the PE samples from backscattering Raman spectroscopy. These bands are associated with the in-phase and out-of-phase C–C stretching modes of all-*trans* conformers, respectively, which may be located either in the crystalline or amorphous phases. The $\langle P_2 \rangle$ and $\langle P_4 \rangle$ coefficients were determined from the intensity ratio of the 1130 and 1060 cm^{-1} bands obtained from backscattering measurements using the calibration curves published elsewhere[24].

Wide-angle X-ray diffraction

In contrast with other characterization methods of the molecular orientation, WAXD can be used to measure the complete orientation distribution of the crystallographic plane normals. It is thus possible to calculate any of the $\langle P_n \rangle$ coefficients for the crystalline phase of the polymer by integration over every possible orientation[25,26]:

$$\langle P_n(\cos\chi) \rangle = \frac{\int_0^{90} I^*(\chi) P_n(\cos\chi) \sin\chi \, d\chi}{\int_0^{90} I^*(\chi) \sin\chi \, d\chi} \quad (8)$$

where $I^*(\chi)$ represents the intensity of diffraction at the polar angle χ. In the case of uniaxial cylindrical symmetry, the $\langle P_n \rangle$ values calculated from different crystal planes can be related to the $\langle P_n \rangle_c$ coefficients corresponding to the crystalline c-axis, which is parallel to the molecular chains, by using[27]:

$$\langle P_n \rangle_c = \frac{\langle P_n \rangle}{P_n(\cos\beta)} \quad (9)$$

where β is the angle between the normal to the considered plane and the c-axis.

For polymers containing only light elements (C, H, O, N), the optimal thickness[28] for WAXD is typically 1–2 mm. However, in practice, samples ranging from a few micrometres to ~1.5 mm can be studied. With thicker samples, a loss of resolution occurs because of the smearing of the diffraction peaks. In this study, the orientation of the PE crystalline phase was calculated from six crystal planes (110, 200, 020, 011, 211 and 002) of the orthorhombic unit cell [$a = 0.741$, $b = 0.492$, c (chain axis) = 0.2538 nm][29,30]. Details on the $\langle P_n \rangle$ calculations from the different crystal planes are given in an earlier publication[19].

EXPERIMENTAL

Samples

The cylindrical rods used in this study were made of Du Pont SCLAIR 2909 high density polyethylene (HDPE) resin (M_n = 16 400, M_w = 56 500). The oriented rods were produced by ram extrusion of preheated billets (120°C) at 145–155°C through conical dies of different diameters. Tension was applied on the samples at the exit of the die in order to obtain straight rods. Translucent rods with λ values of 6, 8, 12, 16 and 20 and with diameters ranging from 13.9 to 7.3 mm were studied. The degree of crystallinity (X_{cryst}) of these rods was determined by density measurements in isopropanol–water mixtures. A milling machine was used to cut 1.2 mm thick platelets in the centre of the rods, along the extrusion direction (*Figure 2A*). For measurements made in the transmission geometry, the use of thick platelets reduces the fraction of surface material, which may be affected by the sectioning process.

The H-shaped moulding reported herein was made of Du Pont SCLAIR E915-06 HDPE resin (M_n = 20 800, M_w = 188 000). It was produced by solid state extrusion of a cylindrical billet at 120°C, followed by rolling. The orientation of the sample was found to be homogeneous along the extrusion axis, but not in the TD and ND. Owing to this inhomogeneity, λ cannot be evaluated. In order to characterize this sample, 1 mm thick platelets were cut along the extrusion direction using a milling machine (*Figure 2B*).

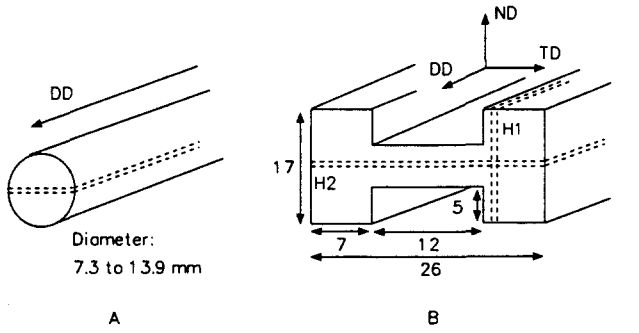

Figure 2 (A) Samples cut along the diameter of cylindrical rods; (B) H1 and H2 platelets cut from an H-shaped moulding (dimensions are given in mm)

I.r. spectroscopy

I.r. spectra were obtained with a Bomem DA3-02 Fourier transform spectrophotometer. The radiation was polarized with a rotating wire-grid polarizer (Specac, UK) mounted in front of the sample. The phase correction and the reference spectrum were measured separately for each polarization. For the orientation measurements, 500 scans were co-added with a maximum optical retardation of 0.5 cm and triangularly apodized to yield a resolution of 2 cm^{-1}. I.r. dichroism was calculated from the peak height intensity measured in absorbance. All spectra manipulations were executed with SpectraCalc software (Galactic Industries Corporation).

Raman spectroscopy

The Raman spectra were recorded with a Spex model 1400 double monochromator computerized spectrophotometer using a Spectra Physics model 2020 argon ion laser tuned at 514.5 nm. Experiments were performed using the backscattering geometry, with the incident light parallel either to the ND or the TD. The polarization direction of the incident beam and the polarization of the analyser were parallel to the DD of the sample. The scattered light was collected with an $f/2$ lens towards the analyser and the polarization scrambler. All spectra were recorded at 21°C with a laser power of 100 mW at the sample, a spectral resolution of 5 cm^{-1}, and an integration period of 2 s by 2 cm^{-1} steps.

The Raman spectroscopy measurements were made on the 1 mm thick PE platelets used in the WAXD and i.r. experiments. However, since the Raman spectra recorded by reflection are very sensitive to surface inhomogeneities, the results obtained on the 'rough' surface prepared by milling were not consistent. It was, therefore, necessary to remove 10 μm of the platelet surface using a microtome (tungsten–carbide blade) before recording the spectra.

X-ray diffraction

WAXD measurements were made using the Ni-filtered Cu Kα radiation (0.15419 nm) produced by a Rigaku rotating anode X-ray generator (Rotaflex RU-200BH) operated at 50–55 kV and 160–190 mA. The collimation was achieved using a Soller slit and a 1.0 mm pinhole. The detection of the diffracted intensity was provided by a scintillation counter coupled with a pulse-height analyser.

All scans were recorded with the symmetrical transmission technique, the normal to the sample surface being positioned at an angle θ with respect to the incident X-ray beam and the detector at an angle 2θ (Bragg angle). During the orientation measurements, the polar angle rotation of the sample (rotation of the sample around the normal to its surface) was performed from $\chi = -90$ to 90° at a rate of 30° min^{-1}, 0° corresponding to the extrusion direction (DD, *Figure 1*). Measurements were taken at 0.5° intervals, using 1.5° and 0.25° slits for 2θ and polar angle resolution, respectively.

RESULTS AND DISCUSSION

Cylindrical rods

The variation of the $\langle P_2 \rangle_c$ coefficient as a function of λ is shown in *Figure 3A* for measurements taken in the centre of the PE cylindrical rods. I.r. dichroism results demonstrate that the crystalline phase of PE (1894 cm^{-1} band) becomes more highly oriented in the DD than the vinyl end groups (909 cm^{-1} band), because the latter groups are mainly located in the amorphous phase where the chains are more disordered than in the crystals[31]. However, previous studies have shown that the $\langle P_2 \rangle_c$ coefficients measured from the 909 cm^{-1} band are higher than those obtained from i.r. bands associated with the carbon backbone in the amorphous phase and, therefore, that the vinyl end groups are not characteristic of this phase[31–33]. This trend was explained by a partial incorporation of the vinyl end groups within the crystal phase or by the emergence of these groups at the crystal surface. The maximum $\langle P_2 \rangle_c$ values measured from the 909 and 1894 cm^{-1} i.r. bands are in close agreement with those reported in the literature for highly oriented HDPE ($\lambda \geqslant 16$)[31,32,34,35].

$\langle P_n \rangle_c$ coefficients characterizing the molecular chain orientation were calculated from WAXD measurements of the 110, 200, 020, 001, 211 and 002 reflections using equation (9), and an excellent correlation was obtained between them[19]. The average values presented in *Figure 3A* correspond very closely to the orientation function calculated from the 1894 cm^{-1} i.r. band, in agreement with previous studies[21,33–35]. The $\langle P_2 \rangle_c$ coefficients measured from this i.r. band and from the X-ray diffraction technique increase rapidly at low λ values to almost reach unity between $\lambda = 8$ and 12, and remain thereafter approximately constant, as it has been reported previously for oriented PE[7,14,19,31–36].

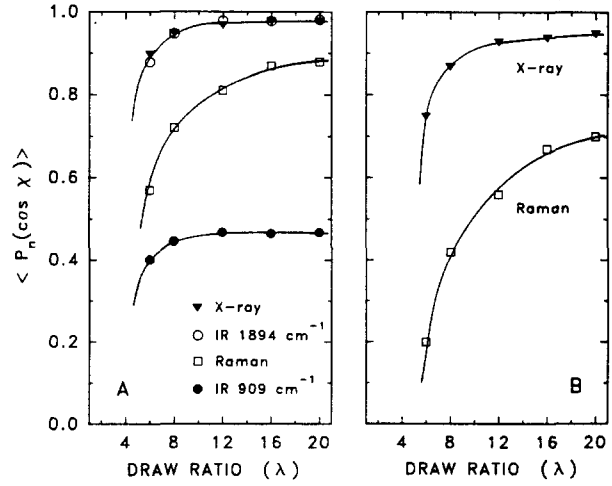

Figure 3 Variation with draw ratio of the $\langle P_n \rangle_c$ coefficients calculated from wide-angle X-ray diffraction, Raman spectroscopy, and from the 1894 and 909 cm^{-1} i.r. bands: (A) $\langle P_2 \rangle_c$; (B) $\langle P_4 \rangle_c$

Table 1 Degree of crystallinity, X_{cryst}, of cylindrical rods of different draw ratios, λ, and $\langle P_2\rangle_{cryst}$, $\langle P_2\rangle_{trans,am}$ and $\langle P_2\rangle_{Raman}$ coefficients characterizing the orientation of all-*trans* C–C bonds in the crystalline phase, in the amorphous phase, and in both phases, respectively

λ	X_{cryst}	$\langle P_2\rangle_{cryst}$[a]	$\langle P_2\rangle_{trans,am}$[b]	$\langle P_2\rangle_{Raman}$
6	0.73	0.89	−0.29	0.57
8	0.75	0.95	0.03	0.72
12	0.79	0.97	0.21	0.81
16	0.78	0.98	0.48	0.87
20	0.79	0.98	0.50	0.88

[a] Average value obtained from X-ray diffraction and from the 1894 cm^{-1} i.r. band
[b] Calculated using equation (10)

In contrast with the preceding results, the $\langle P_2\rangle_c$ coefficient measured by Raman spectroscopy still increases for λ values >12. The values obtained by Raman spectroscopy are lower than those calculated for the crystal phase from X-ray diffraction and from the 1894 cm^{-1} band, but are higher than those determined from the 909 cm^{-1} i.r. band for the vinyl end groups. This intermediate result can be explained by the fact that the 1130 and 1060 cm^{-1} Raman bands are due to the all-*trans* conformers, which are found in both the amorphous and crystalline phases. The $\langle P_2\rangle$ value calculated from these bands thus corresponds to an average over the *trans* C–C bonds located in both phases[24]. Since the coefficients obtained by X-ray diffraction and from the 1894 cm^{-1} i.r. band are constant at $\lambda \geqslant 12$, the increase of the $\langle P_2\rangle$ values measured by Raman spectroscopy at high λ values can be associated with the alignment in the extrusion direction of the *trans* conformers located in the amorphous phase. Assuming a two-phase model, the $\langle P_2\rangle_{trans,am}$ coefficient characterizing the orientation of the *trans* conformers located in the amorphous phase can be calculated by subtracting the crystalline contribution from the coefficient measured by Raman spectroscopy[24], $\langle P_2\rangle_{Raman}$:

$$\langle P_2\rangle_{trans,am} = \frac{\langle P_2\rangle_{Raman} - (X_{cryst}\langle P_2\rangle_{cryst})}{1 - X_{cryst}} \qquad (10)$$

Table 1 gives the $\langle P_2\rangle_{trans,am}$ coefficients obtained from this equation, using the average value of the $\langle P_2\rangle_c$ values measured by X-ray diffraction and by the 1894 cm^{-1} i.r. band as $\langle P_2\rangle_{cryst}$. For the $\lambda = 6$ rod, the $\langle P_2\rangle_{trans,am}$ value is negative, indicating that the *trans* conformers are perpendicular to the DD. At $\lambda = 8$, the $\langle P_2\rangle_{trans,am}$ coefficient is nearly zero, which corresponds either to an unoriented state or to a distribution centred around 55° from the DD [$P_2(\cos\chi) = 0$ for $\chi = 54.7°$]. For the rods of higher λ values, the coefficient becomes positive, showing that the *trans* C–C bonds in the amorphous phase gradually orient towards the extrusion direction. These results are in good agreement with those of Kaito *et al.*, who calculated from measurements of the 2016 cm^{-1} i.r. band the $\langle P_2\rangle_{2016,am}$ coefficient characterizing the orientation of chain segments in the amorphous phase having four or more successive *trans* C–C bonds[34]. For HDPE samples roll-drawn at temperatures above 100°C, these authors obtained $\langle P_2\rangle_{2016,am}$ values near zero at $\lambda \approx 7$, followed by a sharp increase of the orientation up to λ values between 12 and 15 where the coefficient reaches a maximum value between 0.45 and 0.50. The calculation of the $\langle P_2\rangle_{2016,am}$ coefficient by using the $\langle P_2\rangle$ and X_{cryst} values reported by Dupuis *et al.*[33] and Seguela and Rietsch[37] from measurements of the 1894 and 2016 cm^{-1} i.r. bands demonstrates that the evolution of the orientation of the *trans* segments in the amorphous phase of PE depends on the temperature of deformation. For samples drawn at 80°C, a positive $\langle P_2\rangle_{2016,am}$ coefficient is already obtained at $\lambda = 1.4$, which indicates that the *trans* segments orient towards the DD from the onset of the deformation, as it has also been observed by Read and Stein[21] and by Wedgewood and Seferis[38]. However, the dynamic study of the drawing at 110°C shows that relaxation occurs rapidly at this temperature ($\leqslant 30$ ms), and the $\langle P_2\rangle$ coefficient measured at this temperature for the 2016 cm^{-1} i.r. band reaches a maximum value of ~0.55 instead of 0.75 at 80°C[33]. This lower $\langle P_2\rangle$ value has to be ascribed almost entirely to the relaxation of the chains located in the amorphous phase, since the orientation measured for the 1894 cm^{-1} i.r. band is nearly identical for the samples drawn at 80 and 110°C, in accordance with previous experiments which have demonstrated that annealing at $\leqslant 110$°C practically does not influence the crystal phase orientation[31,39]. Taking into consideration that X_{cryst} is reduced to 75% of its room temperature value for the spectra recorded at 110°C[33,37], the $\langle P_2\rangle_{2016,am}$ coefficient that can be calculated at $\lambda = 9$ is ~0.20, which compares well with the Raman spectroscopy results presented in *Table 1*.

The transformation from the lamellar to the fibrillar morphology has been observed to be completed at $\lambda = \sim 8$ for PE[39]. I.r. spectroscopy studies of this transformation have shown that the fraction of *trans* conformations increases at the expense of sequences containing *gauche* bonds in the amorphous phase[32,34,38]. Accordingly, the enhanced mechanical properties of the fibrillar structure in the DD as compared to those of the lamellar structure is ascribed to the presence of extended chains that cross the amorphous layers and act as intra- or interfibrillar tie molecules, which carry most of the axial load in the fibrils[39]. Besides, Kaito *et al.* reported that the increase of the fraction of *trans* sequences is more pronounced for low drawing temperatures[34]. Moreover, the annealing of deformed PE at temperatures above 110°C causes a sharp decrease of the elastic modulus, when the taut tie molecules relax by pulling chain segments from the crystal blocks they are anchored in. The low $\langle P_2\rangle_{trans,am}$ or $\langle P_2\rangle_{2016,am}$ coefficients calculated for *trans* conformers at $\lambda \leqslant 8$ can thus be explained by a rapid relaxation of a large fraction of the chains in the amorphous phase which have been stretched during the transition to the fibrillar morphology. This process is favoured by a high deformation temperature and by a slow cooling of the polymer in the case of specimens with large dimensions.

The high value of the $\langle P_2\rangle_{cryst}$ coefficient measured for the $\lambda = 6$ cylindrical rod indicates that a major fraction of the material has undergone the transformation from the lamellar to the fibrillar structure. At this point, a sharp meridional maximum is observed by small-angle X-ray scattering (SAXS), indicating that the microfibrils are composed of a regular stacking of highly oriented crystal blocks separated by amorphous layers[39]. In the centre of these amorphous layers, the relaxation of the chains should result in a random orientation[40]. However, Petraccone *et al.* have suggested that a barrier effect could lead to an orientation of chain segments parallel to the surface of the crystallites[41], which would explain the

Table 2 Full-width at half-height, $\chi_{1/2}$, of the 002 orientation distribution, and average $\langle P_n \rangle_c$ values calculated from WAXD measurements taken in the centre (C) and at 1 mm from the surface (S) of the cylindrical rods

λ	Rod diameter (mm, ±0.1)		$\chi_{1/2}$ (deg)	$\langle P_2 \rangle_c$	$\langle P_{16} \rangle_c$	$\langle P_{32} \rangle_c$
6	13.9	C	14.0	0.92	0.12	0.01
		S	12.9	0.94	0.18	0.02
8	12.1	C	9.5	0.95	0.36	0.06
		S	8.5	0.96	0.44	0.10
12	9.5	C	6.0	0.97	0.60	0.23
		S	6.0	0.97	0.62	0.26
16	8.2	C	5.0	0.98	0.68	0.35
		S	5.3	0.97	0.64	0.31
20	7.3	C	4.4	0.98	0.72	0.45
		S	5.1	0.97	0.65	0.33

negative $\langle P_2 \rangle_{trans,am}$ measured by Raman spectroscopy at $\lambda = 6$. The drawing of the fibrillar structure to higher λ values yields protrusions of crystalline blocks in the amorphous layers, which reduces the electron density differences between the two components and eventually leads to the disappearance of the SAXS maximum[39]. The displacement of crystal blocks relative to each other causes the tie molecules to become gradually taut and to orient towards the draw direction, as observed by the increase of the $\langle P_2 \rangle_{trans,am}$ coefficient.

The variation of the molecular orientation with λ can also be characterized by the fourth term of the orientation distribution function, $\langle P_4 \rangle$. This coefficient was calculated from Raman spectroscopy and X-ray diffraction measurements using the bands or planes of diffraction mentioned earlier, and the results are plotted in *Figure 3B*. As was observed for the second-order coefficient, the $\langle P_4 \rangle_c$ values calculated from X-ray diffraction show a sharp increase of the crystal phase orientation at $\lambda \leqslant 8$. This rapid variation corresponds to the transformation from the lamellar to the fibrillar morphology. The subsequent deformation of the fibrillar structure induces shearing of the fibrils and their translation relative to each other, which results in a decrease in the width of the orientation distribution. However, this change can hardly be observed by the evolution of the $\langle P_2 \rangle_c$ and $\langle P_4 \rangle_c$ coefficients calculated for the crystal phase, which almost equal unity, because the corresponding Legendre polynomials are broader functions than the orientation distribution obtained after the formation of the fibrillar structure. This is shown in *Figure 3B* by the shape of the X-ray curve, which levels off at $\lambda \geqslant 12$. Nevertheless, Lafrance *et al.* have shown that differences in the orientation of PE crystals at λ values as high as 50 can be characterized through the higher terms of the orientation distribution function, $\langle P_n \rangle$ $(n > 10)$[14,19]. The sensitivity of the higher order coefficients is shown here by the progressive increase up to $\lambda = 20$ of the $\langle P_4 \rangle$ coefficients obtained from Raman spectroscopy, whereas the $\langle P_2 \rangle_c$ curve almost levels off at $\lambda \geqslant 16$. The variation of the $\langle P_4 \rangle_c$ values measured by this latter technique for the rods of high λ values is due to the orientation of the all-*trans* C–C bonds in the amorphous phase.

Table 2 gives average $\langle P_n \rangle_c$ values obtained from X-ray polar scans of the 200, 020 and 002 reflections taken in the centre and at 1 mm from the surface of the rods. For the $\lambda = 6$ and 8 samples, the coefficients measured in the centre are smaller than those measured near the surface of the rods. For $\lambda = 8$, this difference is mainly seen by the narrower width at half-height of the 002 orientation distribution, which results in higher $\langle P_{16} \rangle_c$ and $\langle P_{32} \rangle_c$ values. The $\lambda = 12$ rod is homogeneous through its thickness, while those extruded at $\lambda = 16$ and 20 are slightly less oriented near the surface than in the centre. The higher orientation measured near the surface of the low λ rods could result from a larger shear stress near the die wall during the extrusion. Furthermore, in rods of large diameters, relaxation may be more important during the slow cooling in the centre of the rod than in its outer part which was exposed to air at the exit of the die. The lower orientation near the surface of the $\lambda = 16$ and $\lambda = 20$ rods could be explained by some overheating during extrusion because, in order to obtain these high λ values, the die temperature had to be raised to 155°C, while extrusion was performed at 145°C for the $\lambda \leqslant 12$ rods.

H-shaped sample

Collimation of the incident beam gives a spatial resolution ≤1 mm for the three characterization methods used in this study. It is thus possible to observe sharp variations of the $\langle P_2 \rangle_c$ coefficients measured at different positions on the platelet cut from the H-shaped sample in the DD/ND plane (H1, *Figure 2B*), as plotted in *Figure 4A*. The sample can be divided into three zones. In the central zone ($D = 0$–4 mm), where the material is opaque, the molecular orientation is low and nearly constant. It increases rapidly in the intermediate zone located between $D = 4$ mm and 6 mm, where the sample becomes translucent. For the edges of the sample ($D = 6$–8.5 mm), $\langle P_2 \rangle_c$ values of ~0.45 and ~0.95 are obtained from the 909 cm^{-1} i.r. band and for the crystal phase, respectively. These high values, by comparison to those of *Figure 3A*, indicate that the effective λ is >8 in this region.

For the highly oriented edges, the trends that are

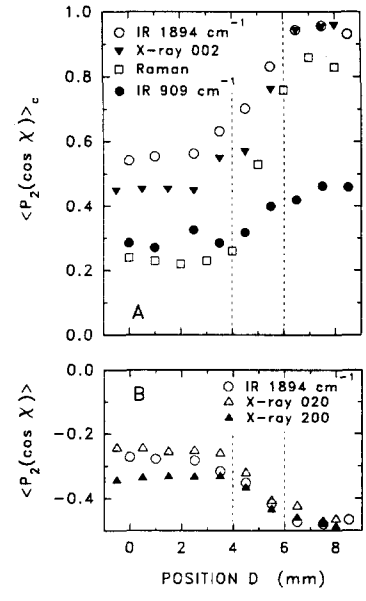

Figure 4 Values of the $\langle P_2 \rangle_c$ and $\langle P_2 \rangle$ coefficients calculated from X-ray diffraction (002, 200 and 020 reflections), Raman spectroscopy and i.r. dichroism (1894 and 909 cm^{-1}) at different positions from the centre of the H1 platelet (see *Figure 2*): (A) $\langle P_2 \rangle_c$; (B) $\langle P_2 \rangle$

observed by comparing the different characterization methods are similar to those reported in the previous section for the cylindrical rods. A good correlation is observed between the $\langle P_2\rangle_c$ coefficients calculated from the 002 reflection and from the 1894 cm^{-1} i.r. band, while the coefficients obtained by Raman spectroscopy values are intermediate between the crystal phase results and those characterizing the vinyl end groups (909 cm^{-1}). In contrast, in the centre of the sample, the $\langle P_2\rangle_c$ values determined by Raman spectroscopy are slightly lower than those obtained from the 909 cm^{-1} i.r. band. This result can be explained by light scattering or depolarization caused by the opacity of the material in this part of the sample. Raman measurements made in this region were not reproducible and the spectra show a poor signal-to-noise (S/N) ratio. Spectra with low S/N ratio systematically lead to low $\langle P_n\rangle$ coefficients, as was observed in reproducibility tests made with the $\lambda=6$ cylindrical rod, which was translucent but slightly more opaque than rods of higher λ values. The values presented herein for the $\lambda=6$ rod were calculated from Raman spectra exhibiting good S/N ratio, which could not be obtained in the opaque central zone of the H1 platelet.

It can also be observed in *Figure 4A* that, in the central and intermediate zones of the H1 platelet, the 002 X-ray results are lower than those measured from the 1894 cm^{-1} i.r. band. This discrepancy arises from the contribution of crystal planes which are not resolved from the 002 peak in the WAXD polar scans of low orientation PE (231, 421, 511, 520, 600 and 040 planes; *Figure 5*). In order to subtract this contribution, curve fitting of the 002 scan was performed, using a Pearson VII function, and the integrals of equation (8) were computed from the curve that gave the best fit in an angular range of 45° from the 002 peak maximum. Nevertheless, it is shown in *Figure 4A* that the $\langle P_2\rangle_c$ values obtained by this procedure, which had been used successfully to eliminate background noise in the 002 polar scans of highly oriented PE[14], are still below the 1894 cm^{-1} i.r. band results. Moreover, the sum of the $\langle P_2\rangle$ coefficients of the *a*, *b* and *c* crystal axes, which were calculated from X-ray diffraction measurements of the 200, 020 and 002 reflections, respectively, is not equal to zero as required by the orthogonality relationship. It is rather observed that:

$$\langle P_2\rangle_c < -(\langle P_2\rangle_a + \langle P_2\rangle_b) \qquad (11)$$

It is thus concluded that the 002 reflection can hardly be used to calculate the chain axis orientation for low orientation PE.

Since the transition moment vector of the 1894 cm^{-1} i.r. band is perpendicular to the molecular chain axis, its $\langle P_2\rangle$ coefficient can be compared directly with the values characterizing the orientation of the *a* and *b* crystal axes. It is observed in *Figure 4B* that the results obtained by i.r. spectroscopy for the crystal phase agree very well with those calculated from X-ray diffraction measurements of the 200 and 020 reflections for the edges of the H1 platelet. For the central region of lower orientation, the $\langle P_2\rangle$ values measured from the 1894 cm^{-1} i.r. band are intermediate between the coefficients calculated from the 200 and 020 planes, as reported by Dupuis *et al.*[33]. However, *Figure 4B* shows a better correlation between the i.r. results and those measured for the *b* axis than with those measured for the *a* axis, in contrast with the results of Dupuis *et al.*, and with those of Read and Stein who have suggested that the dipole moment of the 1894 cm^{-1} i.r. band could be parallel to the *a* axis, because the $\langle P_2\rangle$ values calculated from this band were comparable with those derived from X-ray diffraction measurements of the 200 crystal planes[21]. The discrepancy between the results of *Figure 4B* and those reported by these authors could arise from different deformation mechanisms in HDPE in comparison to the low density PE samples investigated in these previous publications. The fact that the $\langle P_2\rangle$ coefficients obtained from the 200 planes are more negative than those calculated from the 020 planes in the low orientation central zone of the sample (*Figure 4B*) is consistent with the observation that, in the case of melt-crystallized PE, the *a*-axis orientation towards the normal to the DD occurs faster than that of the *b*-axis during the first stages of the deformation ($\lambda \leqslant 3$)[21,33,42-45].

X-ray diffraction polar scans presented in *Figure 5* show that, in the centre of the H1 platelet (D = 1.5 mm), the orientation distribution of the 002 planes is broad and centred along the extrusion/rolling direction. The orientation distribution measured in the intermediate zone, on the white and opaque side (D = 4.5 mm), is slightly narrower than in the central region, but is located at ~10° from the DD. On the translucent side of the intermediate zone (D = 5.5 mm), the orientation distribution narrows down markedly and is still centred at 8° from the DD. Finally, in the highly oriented edges of the sample (D = 7.5 mm), the molecular axis is located at ~5° from the DD. The shift of the orientation distribution away from the DD is probably caused by the transverse flow of the polymer in the rolling process of the H-shaped platelet.

WAXD is the only technique that can be used to locate precisely the position of the molecular orientation distribution with respect to the DD, through the direct measurement of different crystal planes. It must be realized that the $\langle P_2\rangle$ coefficient does not show significant differences for moderate shifts of the orientation distribution position. For example, Lorentzian distributions centred at $\chi=0°$ with full-width at half-height of 8, 15 and 30° give $\langle P_2\rangle$ values of

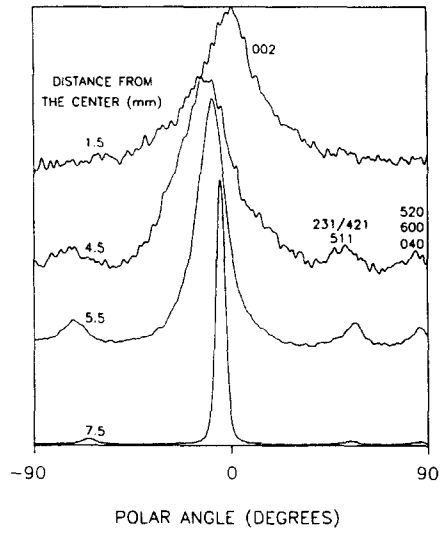

Figure 5 Wide-angle X-ray diffraction polar scans of the 002 reflection measured at different positions from the centre of the H1 platelet. Unresolved reflections contributing to the diffraction are identified on the right-hand side of the figure[19]

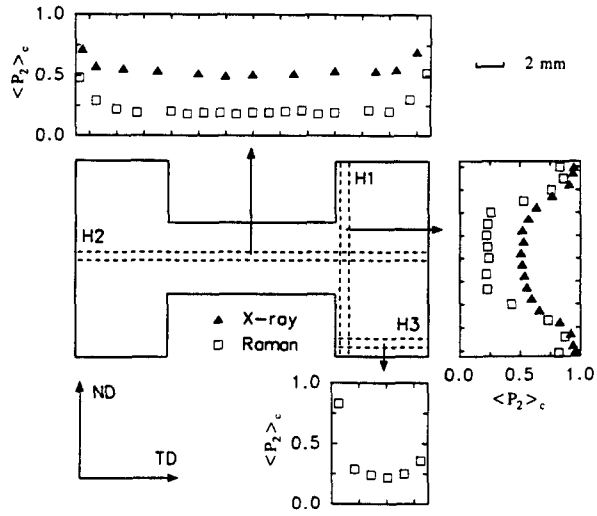

Figure 6 $\langle P_2 \rangle_c$ coefficients measured by X-ray diffraction (110, 200 and 020 reflections) and by Raman spectroscopy at different positions for the H1, H2 and H3 platelets

0.94, 0.85 and 0.67, respectively, whereas coefficients of 0.91, 0.83 and 0.64 are obtained when the distribution maximum is located at $\chi = 10°$. Such shifts of the orientation distribution cause significant variations of the high order $\langle P_n \rangle$ coefficients and can, therefore, be characterized by X-ray diffraction.

Figure 6 shows the orientation profiles measured by Raman spectroscopy and by X-ray diffraction for the H1, H2 and H3 platelets. Measurements made for the 110, 200 and 020 reflections were used to calculate the $\langle P_2 \rangle_c$ values, using equation (9). It is observed that the orientation is higher at ~ 1 mm from the surface of the moulding, whereas low and almost constant $\langle P_2 \rangle_c$ coefficients are obtained in the central zones of the platelets. The highest orientation is measured in the interior of the branches of the H (edges of the H1 platelet), which is the only part of this sample to appear translucent. This result could be explained by the rolling process used, where the material had to flow from the central part of the original cylindrical billet toward the branches. Raman spectroscopy measurements taken on the H3 platelet show that the orientation in the centre of the branch is comparable to that measured for other points located in the bulk of the moulding. As it was discussed for the central zone of the H1 platelet, the $\langle P_2 \rangle_c$ coefficient calculated from Raman spectra taken in opaque regions of these samples may be lower than the actual value because of light diffusion or depolarization. Nevertheless, the coherence between the X-ray diffraction and the Raman results presented in *Figure 6* indicates that this latter technique can be useful to detect variations in the degree of orientation through the thickness of a sample.

CONCLUSIONS

The molecular orientation of thick PE samples was investigated by WAXD, i.r. dichroism and Raman spectroscopy. The original samples were cut by milling to provide ~ 1 mm thick platelets suitable for transmission X-ray diffraction and i.r. spectroscopy. The use of thick platelets increases the amount of bulk material with respect to that of the surface material, which can be affected by the cutting process or which may possess a different orientation as a result of the production process itself (polymer skins)[46]. Investigations of the variation of the orientation through the thickness of the samples were made, with a spatial resolution of 1 mm. Extruded cylindrical rods of λ values ranging from 6 to 20 were found to be quite homogeneous, whereas large differences in orientation were observed for an H-shaped moulding produced by extrusion and rolling.

For the PE crystal phase of the cylindrical rods and of the highly oriented edges of the H1 platelet, an excellent correlation was established between the $\langle P_2 \rangle_c$ coefficients calculated from different X-ray reflections and from the 1894 cm^{-1} i.r. band. In regions of lower orientation, the results obtained from the 1894 cm^{-1} i.r. band compare well with those derived from the 110, 200 and 020 crystal planes. However, the $\langle P_2 \rangle_c$ values calculated from the latter measurements are bigger than the $\langle P_2 \rangle_{002}$ coefficient, even when curve fitting is used to subtract the contribution of unresolved reflections to the 002 orientation distribution.

The 909 cm^{-1} i.r. band showed that the vinyl end groups, which are located mostly in the amorphous phase, orient to a lower extent than the crystals. For λ values >4, the ratio of the $\langle P_2 \rangle_c$ coefficients calculated for the 909 cm^{-1} i.r. band and for the crystal phase lie between 0.45 and 0.55, respectively, as it was previously observed by Glenz and Peterlin[31,32] and by Dupuis *et al.*[33].

The Raman spectroscopy measurements of the orientation of the all-*trans* C–C bonds give $\langle P_2 \rangle$ values that are intermediate between those obtained for the crystal phase and those of the vinyl end groups. One interesting feature of the Raman results is the evolution of the $\langle P_2 \rangle$ and $\langle P_4 \rangle$ coefficients at $\lambda \geqslant 12$, while the crystal phase and vinyl end group orientation has reached a constant value. This increase is explained by the stretching of the tie molecules of the fibrillar morphology of the highly drawn samples. Raman spectroscopy could allow the characterization of the orientation of large polymer specimens without sectioning them, because the measurements are made by reflection. However, this technique is very sensitive to surface roughness, and it was necessary to remove a 10 μm slice from the platelets prepared by milling in order to obtain reproducible spectra. Moreover, birefringence or light depolarization occurring for opaque samples lead to spectra with poor S/N ratios, from which low $\langle P_n \rangle_c$ values are obtained, by comparison to coefficients calculated by other methods.

ACKNOWLEDGEMENTS

This work was made possible through financial support from the Ministère de l'Education du Québec (Fonds FCAR and Action Structurante), the Natural Sciences and Engineering Research Council of Canada and from Alcan International Co. We also thank the Polymer Research group of the Alcan R&D Centre in Kingston for the preparation of the cylindrical rods and the H-shaped moulding.

REFERENCES

1 Ward, I. M. (Ed.) 'Structure and Properties of Oriented Polymers', Applied Science, New York, 1975
2 White, J. L. and Cakmak, M. in 'Encyclopedia of Polymer Science and Engineering' (Eds H. Mark, N. Bikales, C. Overberger and G. Menges), Vol. 10, 2nd Edn, J. Wiley & Sons, New York, 1987, pp. 595–636

3 White, J. L. and Spruiell, J. E. *Polym. Eng. Sci.* 1983, **23**, 247
4 Maddams, W. F. and Preedy, J. E. *J. Appl. Polym. Sci.* 1978, **22**, 2721
5 White, J. L. and Spruiell, J. E. *Polym. Eng. Sci.* 1981, **21**, 859
6 Yoda, O. and Kuriyama, I. *J. Polym. Sci., Polym. Phys. Edn* 1977, **15**, 773
7 Kaito, A., Nakayama, K. and Kanetsuna, H. *J. Appl. Polym. Sci.* 1985, **30**, 1241
8 Krause, S. J. and Hosford, W. F. *J. Polym. Sci., Polym. Phys. Edn* 1989, **27**, 1867
9 Dhingra, V. J., Spruiell, J. E. and Clark, E. S. *Polym. Eng. Sci.* 1981, **21**, 1063
10 Sakai, Y. and Miyasaka, K. *Polymer* 1988, **29**, 1608
11 Kyu, T., Fujita, K. and Cho, M. H. *Polym. Eng. Sci.* 1989, **29**, 383
12 Gerrits, N. S. J. A., Young, R. J. and Lemstra, P. J. *Polymer* 1990, **31**, 231
13 Ishikawa, K., Miyasaka, K. and Maeda, M. *J. Polym. Sci. A2* 1969, **7**, 2029
14 Lafrance, C. P., Debigaré, J. and Prud'homme, R. E. *J. Polym. Sci., Polym. Phys. Edn* 1993, **31**, 255
15 Ward, I. M. (Ed.) 'Developments in Oriented Polymers', Applied Science, London, 1982
16 Samuels, R. J. 'Structured Polymer Properties', Wiley-Interscience, New York, 1974
17 Hermans, J. J., Hermans, P. H., Vermaas, D. and Weidinger, A. *Rec. Trav. Chim. Pays-Bas* 1946, **65**, 427
18 Hermans, P. H., Hermans, J. J., Vermaas, D. and Weidinger, A. *J. Polym. Sci.* 1947, **3**, 1
19 Lafrance, C. P., Pézolet, M. and Prud'homme, R. E. *Macromolecules* 1991, **24**, 4948
20 Jasse, B. and Koenig, J. L. *J. Macromol. Sci. Rev. Macromol. Chem.* 1979, **C17**, 61
21 Read, B. E. and Stein, R. S. *Macromolecules* 1968, **1**, 116
22 Bower, D. I. *J. Polym. Sci., Polym. Phys. Edn* 1972, **10**, 2135
23 Bower, D. I. *J. Phys. B* 1976, **9**, 3275
24 Pigeon, M., Prud'homme, R. E. and Pézolet, M. *Macromolecules* 1991, **24**, 5687
25 Deas, H. D. *Acta Crystallogr.* 1952, **5**, 542
26 Krigbaum, W. R. and Roe, R. J. *J. Chem. Phys.* 1964, **41**, 737
27 Lovell, R. and Mitchell, G. R. *Acta Crystallogr.* 1981, **A37**, 135
28 Alexander, L. E. 'X-Ray Diffraction Methods in Polymer Science', R. E. Krieger, Malabar, 1979
29 Bunn, C. W. *Trans. Faraday Soc.* 1939, **35**, 482
30 Walter, E. R. and Reding, F. P. *J. Polym. Sci.* 1956, **21**, 561
31 Glenz, W. and Peterlin, A. *J. Polym. Sci. A2* 1971, **9**, 1191
32 Glenz, W. and Peterlin, A. *J. Macromol. Sci. Phys.* 1970, **B4**, 473
33 Dupuis, J., Legrand, P., Seguela, R. and Rietsch, F. *Polymer* 1988, **29**, 626
34 Kaito, A., Nakayama, K. and Kanetsuna, H. J. *Macromol. Sci. Phys.* 1987, **B26**, 281
35 Miller, P. J., Jackson, J. F. and Porter, R. S. *J. Polym. Sci., Polym. Phys. Edn* 1973, **11**, 2001
36 Gao, P., Mackley, M. R. and Nicholson, T. M. *Polymer* 1990, **31**, 237
37 Seguela, R. and Rietsch, F. *Polymer* 1986, **27**, 532
38 Wedgewood, A. R. and Seferis, J. C. *Pure Appl. Chem.* 1983, **55**, 873
39 Peterlin, A. *Colloid Polym. Sci.* 1987, **265**, 357
40 Mandelkern, L. *J. Polym. Sci. Symp.* 1973, **43**, 1
41 Petraccone, V., Sanchez, I. C. and Stein, R. S. *J. Polym. Sci., Polym. Phys. Edn* 1975, **13**, 1991
42 Stein, R. S. *J. Polym. Sci.* 1959, **34**, 709
43 Hay, I. L. and Keller, A. *Kolloid-Z. Z. Polym.* 1965, **204**, 43
44 Matsuo, M., Hirota, K., Fujita, K. and Kawai, H. *Macromolecules* 1978, **11**, 1000
45 Pietralla, M. *Colloid Polym. Sci.* 1976, **254**, 249
46 Mirabella, F. M. *J. Polym. Sci., Polym. Phys. Edn* 1984, **22**, 1293